Siberian Branch of Russian Academy of Science

BUDKER INSTITUTE OF NUCLEAR PHYSICS

V.L. Auslender, A.V. Bulatov, L.A. Voronin,
D.S. Kolesnikov, E.N. Kokin, G.S. Krainov,
A.N. Lukin, A.M. Molokoedov, V.M. Radchenko,
N.D. Romashko,

TECHNIQUE OF DESIGN
AND CALCULATION
OF EXTRACTION DEVICES
FOR ELECTRON ACCELERATORS

Budker INP 2004-27

Novosibirsk
2004

Technique of design and calculation of extraction devices for electron accelerators

V.L. Auslender, A.V. Bulatov, L.A. Voronin, D.S. Kolesnikov, E.N. Kokin, G.S. Krainov, A.N. Lukin, A.M. Molokoedov, V.M. Radchenko, N.D. Romashko

Budker Institute of Nuclear Physics
630090, Novosibirsk, Russia

Abstract

In this paper we considered the problems of design and calculation of the beam extraction devices for electron accelerators taking into consideration the character of interaction of the pulse magnetic fields with the metal walls of the scanning vacuum chambers. We considered the samples of the beam extraction devices and problems of forming of the beam scanning and obtaining the necessary dose fields.

Методика расчета и конструирования выпускных устройств для ускорителей электронов

В.Л. Ауслендер, А.В. Булатов, Л.А. Воронин, Д.С. Колесников, Е.Н. Кокин, Г.С. Крайнов, А.Н. Лукин, А.М. Молокоедов, В.М. Радченко, Н.Д. Ромашко

Институт ядерной физики им. Г.И. Будкера
630090, Новосибирск, Россия

Аннотация

В работе рассмотрен комплекс вопросов, связанных с разработкой и проектированием выпускных устройств ускорителей электронов с учетом особенностей взаимодействия импульсных магнитных полей сканирующих магнитов со стенками вакуумных камер выпускных устройств. Подробно описаны варианты конструкции выпускных устройств. Рассмотрены вопросы формирования развертки пучка и получения дозных полей необходимой конфигурации.

Introduction

By the present time, at BINP quite a large series of electron accelerators have been developed. For the extraction of an electron beam into atmosphere, in each of such devices, the accelerated beam is scanned along the required size of the object under irradiation. To this end, it is used a triangular metal vacuum chamber-bellhood with the scanning magnet at the vertex of the triangle and the extraction window or gamma-converter are placed at the opposite side. These devices are well described elsewhere in literature [1,2,3]. However, the tougher and tougher requirements to the dose field uniformity caused the necessity in more thorough studies of the processes occurred in metal walls of vacuum chambers of the scanning magnets, active losses from the scanning fields, beam turn at the edges of the extraction device as well as consideration of problems related to the development and design of the extraction device using only metal sealings. The presented work (on the example of the development of two extraction devices for the accelerators ILU-10 and KAERI Super conducting Electron Accelerator (KSEA) - (R.Korea) covers all the design problems of the extraction devices.

Basic parameters of these devices are given in the Table 1.

Table 1

Accelerator	ILU-10	KSEA
Power, kW	50	100
Energy, MeV	5	10
Pulse duration	0.5 ms	100 ps
Repetition rate, Hz	50	5 000 000
Average current, mA	10	10

In the first part of the paper we considered the processes occurred in the metal walls of the scanning vacuum chambers in the case they are crossed with the pulse magnetic fields. In the second half of the paper we considered the problems related to the requirements of the dose field uniformity for these accelerators. The third part of the paper is devoted to the design of extraction devices. The fourth part is devoted to the problems of the beam longitudinal scanning and the fifth chapter considers the electron-optical aspects of the beam extraction devices.

1. The main processes occurred in the metal walls of scanning vacuum chambers

1.1 Shielding of the pulsed magnetic fields with the metal cases

When the pulsed magnetic field is applied to the nonmagnetic case of the scanning system, which separates by vacuum the beam deflection space and the outer scanning magnet that could be of different geometric shape, the induced current reactions are occurred. The vortex currents in the depth of the metal shell flow along the elementary turns in the planes perpendicular to the intensity vector of the exciting magnetic field. The current density of each turn is determined by the Faraday law:

$$\oint E dl = -\mu_0 \frac{d}{dt} \iint H dS \ , \tag{1.1}$$

where E is an induced field producing the electric current of density $j = \sigma \cdot E$. H is the magnetic field strength, σ is the case conductivity. Depending on the frequency spectrum of the magnetic field incident onto the shell, for the sake of calculation convenience, one can introduce the term of two frequency regions for shielding this field. These regions are determined the ratio of the skin-layer value to the thickness of the nonmagnetic metal wall of the scanning vacuum chamber. At high frequencies, the current expulsion occurs to the shell wall surface (the surface effect). At low frequencies, there is no such effect and the case behaviour is similar to that of a short-circuited loop. The stainless steel, whose skin-layer thickness at a frequency of 50 Hz is 60 mm and for 1000 Hz it is 13 mm, is used for production of the vacuum chamber walls. In this case, the characteristic time of the field penetration into stainless steel for the used thickness of the order 0.5 – 1 mm is 5 mks. Naturally, for the characteristic scanning frequencies lower that 1 kHz, the surface effect is negligible and the case can be considered as a short-circuited loop, whose wall resistance coincides with the DC resistance. Therefore, the electric circuit of the scanning magnet can be presented in the form of two magnetically connected coils, magnet inductance and a closed loop of the scanning case. The presence of the short-circuited secondary circuit with the presence of current in the magnet winding causes the occurrence of the inverse current, which de-magnetizes the scanning space. Therefore, the total magnetic flux of the scanning will be equal to the difference between the magnetizing flux of the magnet coil and that of the short-circuited loop. The case short-circuited loop decelerates the growth of the scanning magnetic field passing through the wall.

1.1.1 The basic relations for obtaining the required magnetic fields in the scanning devices are the following

As it follows from [4], the field inside the case $H0$(t) is a superposition of the affecting field $H1$(t) and the field $H2$(t), which is excited by currents induced in the shell depth by a pulse $H1(t)$. It is also derived that the field inside the case $H0$(t), which is excited by a pulse $H1$(t), satisfies the ordinary differential equation:

$$H1(t) = \frac{L2}{R2} \cdot \frac{dH0}{dt} + H0(t), \quad H0(0) = 0, \tag{1.2}$$

where $L2$ and $R2$ are the case inductance and its active resistance. Let us give a real example of the calculation technique used for calculations of fields in the scanning devices. For example, we need to obtain in a cosine-shaped vacuum part of the scanning a magnetic field $H0$(t) with the growth time of 0.5 ms. From the equation (1.2) one can determine the value and shape of the exciting field $H1$(t). The ratio $R2/L2$ of time constant of the case circuit remains to be unknown. For finding out this ration, the following scheme is suggested (see Fig.1). Where $L1,L2$ and $R2$ are the scanning components. After commutation and passage of a current half-a-wave, the diode $D1$ cuts the primary circuit and an energy stored in $L2$ falls down from the sought constant $L2/R2$. Since for the ILU-10 type accelerator case this time is 100 mks, and for KSEA, it was taken the case developed for the ELV-series accelerator, the constant value was 250 mks. The field fall down is measured with an induction counter in the form of the flat frame inside the scanning chamber. Fig.2 shows the electric circuit of the scanning magnet power supply. A set of equations for the circuit currents of these two circuits are given below:

$$\left. \begin{array}{l} R1i1 + L1\dfrac{di1}{dt} + M\dfrac{di2}{dt} = E1(t), \\[2mm] R2i2 + L2\dfrac{di2}{dt} + M\dfrac{di1}{dt} = 0. \end{array} \right\} , \tag{1.3}$$

where $L1$ is an inductance of a magnet without case, and $E1(t)$ is a form of the sought e.d.f. that will provide the required fields in the scanning. For the solution of this system of equations, two more parameters of connected circuits as the coupling coefficient and the $L2$ case inductance value remained to be found out.
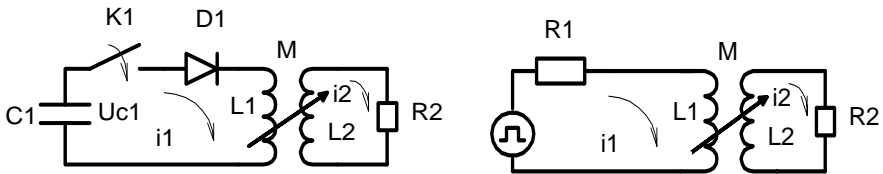
Fig. 1. Scheme for determining *L2/R2*   *Fig. 2*. The magnet power supply circuit.

From the theory of connected circuits [6] it is known that under condition of small-
ness of *R2*, which is evident for the metal cases, the circuit coupling coefficient is equal to:

$$k = \sqrt{\frac{L1 - L1^*}{L1}},\qquad\qquad (1.4)$$

where *L1 is* the magnet inductance without bellhood, *L1** is the magnet inductance in an operative assembly. The coupling coefficient with the ILU-10 case is 0.51 and for KSEA it is 0.64.

    An estimate of the secondary circuit parameters was carried out at the prototype analogue of the scanning vacuum chamber with a simple geometry, which allows to determine easily the dynamic values of the inductance and resistance of the scanning metal shells. Generally speaking, as is shown in [4], the replacement of the case of a complex form by the short-circuited loop is incorrect due to the mutual inductance of various components of the bellhood throat as the cylindrical surfaces, flat parts of the case, etc. However, the authors suggested the replacement of the casing by the volumetric short-circuited loop made of copper bus whose shape repeats the path of a current induced in the metal case. Fig.3 shows the shape of the ILU-10 case and its equivalent. The criterion of equivalence of the vacuum case and its model is the equivalence in the value and form of the field inside the model as well as an approximate equality of the coupling coefficient of the magnet coil and that of the model, which was equal to 0.47. Evaluation of the inductance was performed with the resonance method by the connection to the cut side part of the model capacitance. For the capacitance *C2* = 30 mkF, the resonance frequency was 55,5 kHz and the value of the secondary circuit inductance *L2* = 0.29 mkH. Resistance of *R2* = 0.003 Ohm is selected from the time constant value of the   ILU-10 casing. The model experiments have shown that the volumetric circuit selected with the concentrated parameters *L* and *R* are practically completely imitating the casing, therefore the values *L2* and *R2* are the dynamic characteristics of the scanning vacuum casing.
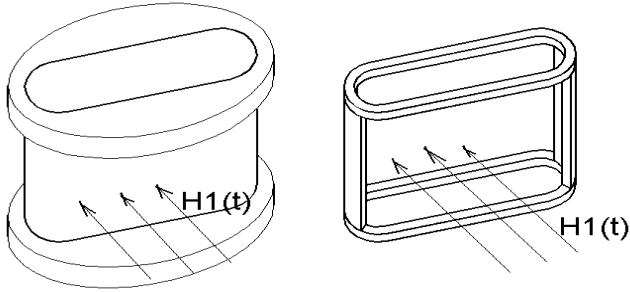
Fig. 3. The outer views of the ILU-10 scanning case and its model.

In conclusion, it is worth mentioning that finding out of *L2* and *R2* exact values is necessary for determining the active losses in the scanning case. This paper does not dwell on determining active losses in the scanning metal shells, though it is worth mentioning that knowing all the dynamic parameters of the secondary circuit, is not complicated. One should only take into account the real paths of the secondary current, information of which is given detailed enough in Ref.4.

The main relations for the exciting field and scanning field in vacuum are determined only by the ratio *L2/R2*, the method of exact determining of which was given above.

By finding out all the parameters of connected circuits and taking into account that $M = k\sqrt{L1L2}$ one can solve the equation (1.2). By finding out *H1(t)* and *H2(t)*, in case of *H2(t) = H1(t) – H0(t)*, it is evident that *H1(t) ~ i1(t),* and *H2(t) ~ i2(t)* , therefore, one can find out the function *E1(t)* from the first equation (1.2). It is natural that the scale coefficients of the real values *H1max* and *i1max* are selected from the design electron-optical considerations and the total current law. Fig.4 shows the design forms of the fields and currents for the LIU-10 case parameters.
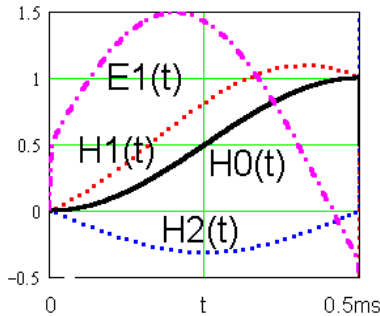
Fig.4. The design values of fields and currents for obtaining the given *H0(t)*.

For the experimental test of that given above, the circuit was made with a discharge of capacitance to the magnet inductance. The set of equations for such a circuit takes the form:

$$\left. \begin{aligned} R1i1 + L1\frac{di1}{dt} + M\frac{di2}{dt} + Uc = 0, \\ R2i2 + L2\frac{di2}{dt} + M\frac{di1}{dt} = 0. \end{aligned} \right\} \tag{1.5}$$

After transformation, we get the differential equation with a single unknown:

$$\frac{d^3i1}{dt^3} + \frac{R1L2 + R2L1}{L1L2 - M^2} \cdot \frac{d^2i1}{dt^2} + \frac{L2 + C1R1R2}{C1(L1L2 - M^2)} \cdot \frac{di1}{dt} + \frac{R2}{C1(L1L2 - M^2)} \cdot i1 = 0 \ , \tag{1.6}$$

in this case, the initial conditions $i1(0), i1'(0), i1''(0)$ for this equations are determined from the known analytic solution of applying such connected circuits to the constant e.d.f. [7]. Fig.5 shows the oscillograms obtained both by calculations and experimentally for the ILU-10 case.
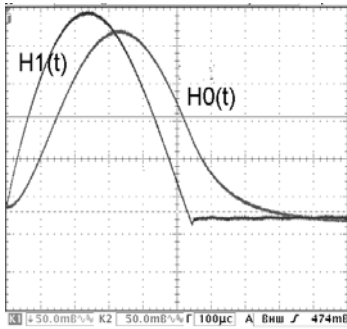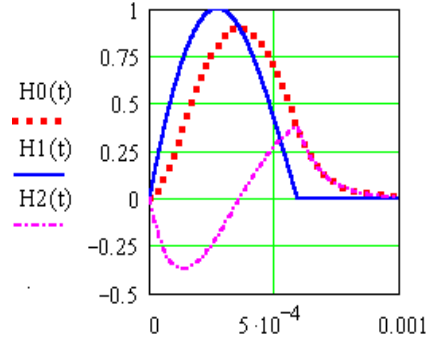
Computation   Experiment

Fig. 5. Field and current curves at discharge of a capacitance to the ILU-10 scanning magnet.

2. Formation of the dose fields at the output of extraction device

2.1 Schematic of producing the gamma-radiation field of ILU-10 accelerator

As an electron-optical model of the extraction device we have selected a scheme that consists of two electromagnets, which are scanning an electron beam in two mutually perpendicular planes and located near the extraction device of the flat quadrupole lens (Panoffsky lens). Fig.6 shows the design electron trajectories in the bellhood plane for three values of the scanning magnetic including the zero value. The change of the beam linear dimensions depending on bias value are determined by the energy spectrum of the ILU-10 accelerator beam whose value

reaches 0.5 MeV at maximum energy of 5 MeV. Its is seen that the current linear density along the extraction length varies substantially depending on the place of the extraction window - lines (a,b,c) and at the fixed position of the foil frame will also be changed depending on the field value in the output quadrupole lens. Fig.7 shows the design values of the current linear density (for the bellhood half) depending on geometry (a,b,c) and values are normalized by the current density without a bias. One should mention that the Panoffsky lens de-focuses the beam along the narrow part of the bellhood uniformly along the whole length of the bellhood. This enables one to superpose the linear density and current density values. This property of the flat quadrupole lenses, in addition to the basic designation of such devices as the post-bending of a beam with respect to the extraction normal, enables one to increase the beam transverse size.
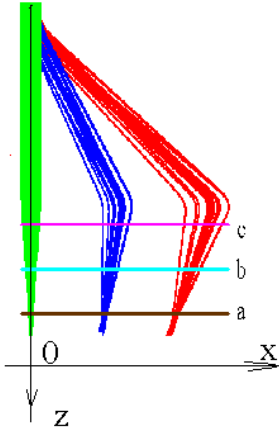
Fig. 6: ILU-10 beam trajectory
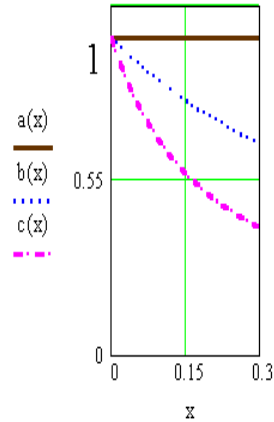
Fig. 7: Current density distribution along the length of ILU-10 bellhood half-length.

In the ILU-10 accelerator, each pulse of an electron beam is scanned through the whole length of a bellhood. This is related with a high energy in a pulse of 1 kJ. The current pulse length is 500 mks. From the evident physical considerations, for obtaining the uniform dose along the extraction device length, the scanning velocity function should repeat the distribution form of the current density along the bellhood length. Shifting to the time coordinates, we obtain the form of the required magnetic fields in vacuum for crossections separated earlier. Fig.8 shows these values $H0(t)$ for versions (a,b,c). As was considered earlier in detail, the given forms of the scanning fields can be obtained under action of the external exciting field $H1(t)$. The values of these fields are related by the equation (1.2).

Fig.9 shows the form of the required external magnetic fields of the scanning generator $-H1(t)$.
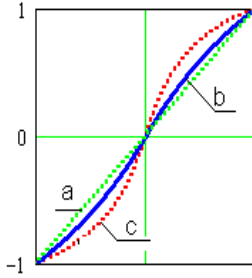
Fig. 8. Form of magnetic field

–

H1(t).
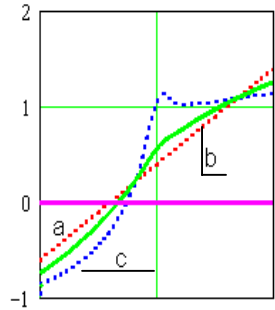
Fig. 9. Field outside the throat

in vacuum – H0(t).

It is worth mentioning again that the external and internal casing fields should be formed by the generator beforehand and at the moment of the current onset should have the required initial conditions as the current value and its derivative. These conditions pose the basic requirements for the design of the power supply systems for the scanning magnet. It is evident that such a device for ILU-10 should comprise its own power supply, its own system of synchronization, etc. Ref.7 shows that the best characteristics of the dose gamma-field behind the converter are obtained at weakly convergent beam of electrons at the target (from the normal minus 6 grades) and with a quadratic growth of the falling down dose at the bellhood edges.

The growth of the electron dose should correspond to the expression

$$\frac{dW}{dx} = 1 + 0.2\left(\frac{x}{x0}\right)^2$$, where x0 = 0.35m, x – coordinate from the converter middle.

Fig.10 shows the forms of the magnetic field in vacuum and exciting field at the casing for this case. The version (b) in Fig.6 was chosen to be the basis of the current density distribution over the converter. This choice was determined by the design considerations from the geometry of the Panoffsky lens installation and the required width of the dose field as well as the optimum use of the bellhood dimensions.

12
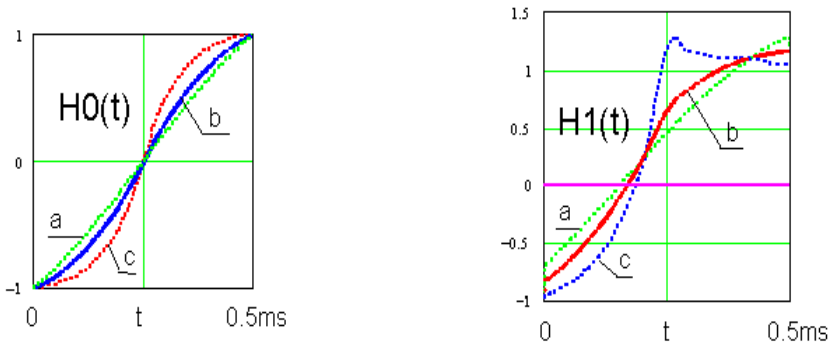
Fig. 10. Design forms of *H0(t)* and *H1(t)*.

For obtaining the given dose distribution we find out the magnetic field forms outside and in vacuum part of the scanning (Fig.10). For the selected version (b) – solid curve in Fig.10, the circuit forming the required current in the magnet winding has been developed. This circuit is power supplied by the forming line of the ILU-10 basic modulator. As was mentioned earlier, when applying the voltage rectangular pulse to the scanning magnet, the inner field cannot contain the jump and starts always from zero and from the zeroth derivative. Fig. 11 shows the oscillogram of the accelerator exciting field.
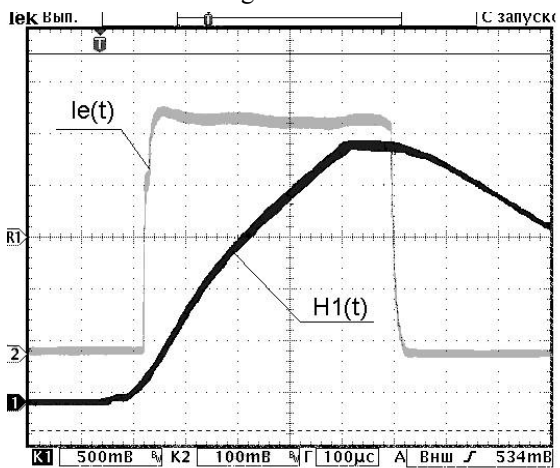
Fig. 11. Oscillogram of the fields *H1(t)* and *Ie(t)*.

The magnet winding is supplied beforehand by the direct current up the maximum deviation value to one side of the bellhood. Fig.12 shows the basic circuit of the scanning magnet power supply from the ILU-10 modulator forming line.

13
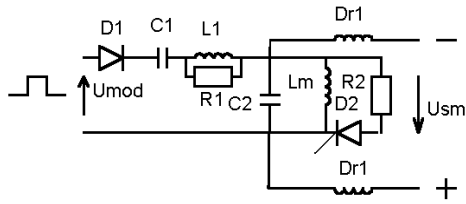
Fig. 12. Electric circuit for power supply of the bending magnet from the ILU-10 modulator.

Let us give a short description of the main components of the scanning power supply circuit. Capacitance *C2* adjusts the form of the scanning field onset. The chain *C1,L1,R1* and *Lm* forms the central part of the scanning field. A decrease in the field growth at the pulse end is achieved by switching with the shunting circuit *R2* and synchronized thyristor line *D2*. The magnet winding *Lm* is power supplied with dc current from the source *Usm* through two similar chokes *Dr1*. Realization of the scheme enabled us to obtain the required distribution of the gamma radiation dose behind the converter, the motion speed of the transverse line with dosimetric films was 1 mm/s at a beam power of 50 kW. By technical conditions, the dose nonuniformity along the entire length of irradiation *L*=0.6 m did not exceed ± 5%. Fig.13 show the photo picture of the ILU-10 extraction device and the power supply of the vertical scanning magnet in the pilot version.
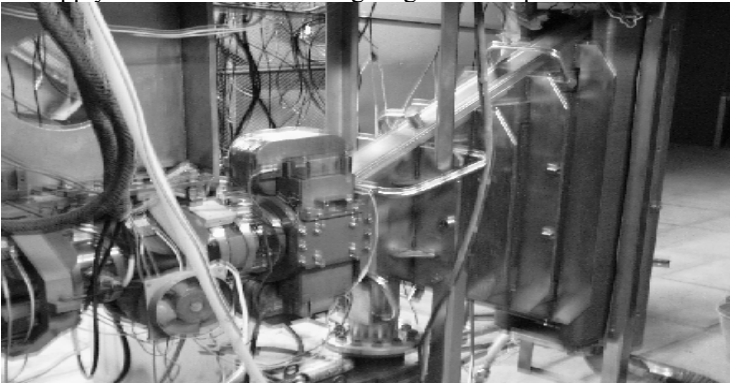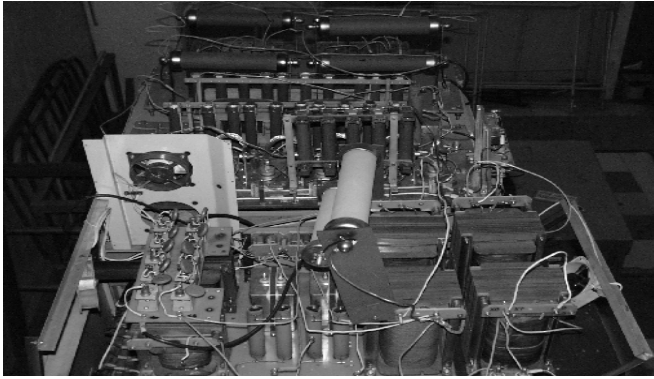
Fig.13. Bellhood of ILU-10 and its pulse power supply systems.

2.2 Scheme of raster formation for electron radiation of KSEA accelerator

The well know scheme of the beam scanning in two mutually perpendicular direction is used for extraction of an electron beam from the vacuum chamber of the KSEA accelerator through the titanium foil. The scanning frequencies were chosen (similarly to [1,2]) in proportion 251/15 that enables one to have the complete feeling of the required radiation raster 600×40 mm without overlapping of the beam trajectories over each other. At low frequency of 50 Hz, the beam is deflected along the foil and at high frequency of 837 Hz, the beam is deflected across. The KSEA accelerator generates a practically monochromatic beam $\Delta E \leq 1\%$ with such a high repetition rate (up to 5 MHz) that from the scanning viewpoint it can be considered as continuous. The beam size is formed by the quadrupole lenses of the supply channel to the size ~1 cm. Scanning electromagnets are fed with the saw like currents. From the viewpoint of the scanning chamber shell influence on the raster form at the extraction foil, the design forms of beam traces on the foil with an account for the metal walls and for the saw with no distortions given in Fig.4 are significant.
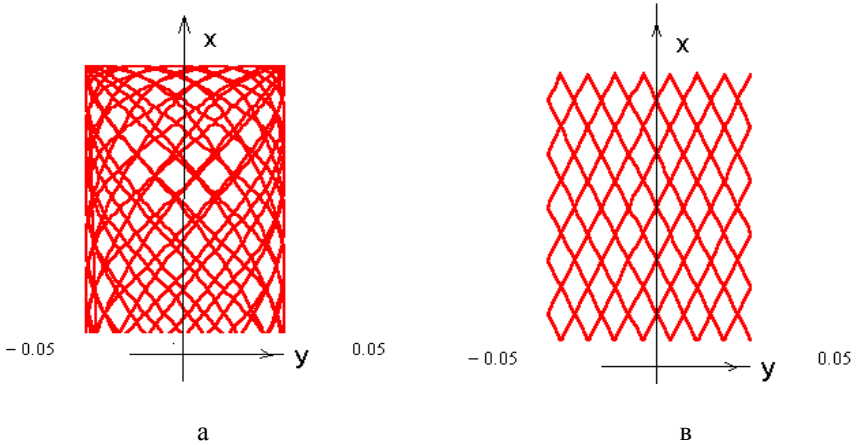
Fig. 14. Raster at the foil end with an account for the influence of the scanning shell (a) and without shell (b).

It is evident that distortions formed by the shell parasitic currents especially for the transverse scanning lead to the noticeable distortions of the uniform density of the extracted current. The calculation of the exciting field *H1(t)* was performed for the measured values of the time constant *L2/R2* = 0.25 ms. If the transverse scanning magnet is supplied with a current of the form *H1(t),* the field in vacuum acquires the ideal saw form and the current density on the foil is balanced.
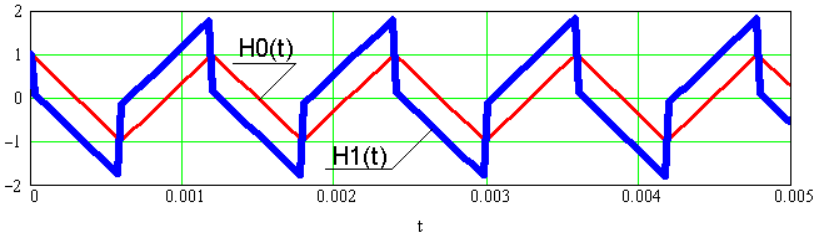
Fig. 15.

Fig.15 shows the forms of fields *H1(t)* and *H0(t)*. At present, for the required power supply system is being developed for the transverse scanning. The scanning along the foil is achieved by the saw wise current with a low frequency 50 Hz whose form is not practically distorted in the presence of the metal vacuum shell.

3. Design of extraction devices

3.1 Extraction device with gamma-converter for ILU-10 accelerator

Fig.16 shows the design of extraction device with the gamma-converter . The triangular vacuum chamber-bellhood **1** is hanged on the bracket **2.** The input rectangular flange of the chamber is connected to the O-shaped chamber **5** to be further referred to as the scanning chamber. The bellhood rectangular flange is shut by the duralumin plate **9** with the size $125 \times 1400mm^2$, which serves as the gamma-converter. The ion sputtering pump NORD-100 **10** is fixed to the bellhood from below. The sylphone connection is installed on the extraction device. **3**. All the All the abovementioned units of the device are vacuum tight connected with the indium wire of 0.8 mm in diameter. Outside the thin-wall chamber there is a
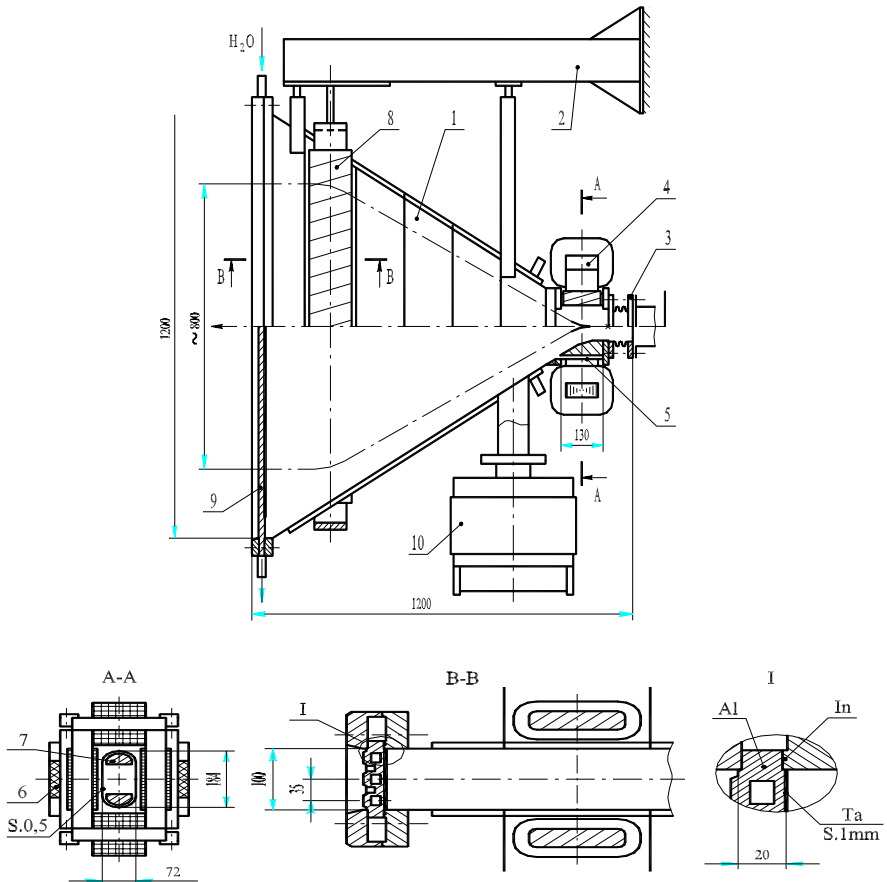
Fig. 16. Extraction device for the ILU-10 accelerator.

scanning magnet **4** with two pairs of coils (see crossection A-A). $\varnothing$ 0,8 mm. The Panoffsky lens **8** is installed outside the bellhood at a distance of 150 mm from the gamma-converter. For protection of the extraction device from radiation reflected from the converter, the water-cooling was arranged for the bellhood walls and the input flange.

It is worth to dwell specially on the design of the scanning chamber loaded by the atmospheric pressure. The chamber has rigid flanges connected with the oval (in transverse crossection) thin-wall shell made of 0.5 mm thick stainless steel 12X18H10T. Additional flanges of the chamber are fixed with two fiberglass supports **6**, which takes the axial load of the atmospheric pressure and serve as a support for the scanning magnet of 65 kg in weight. The accepted wall thickness of 0.5 mm is determined by the requirements of the minimum attenuation of the scanning magnetic field and minimum heating of walls by the whirling currents. At the accepted sizes of the chamber (length l = 130 mm, width – 184 mm, thickness – 72 mm) the sag f in the middle of the chamber flat part was 3 mm to each side. At the length of l = 130 mm, the following radius of cylindrical surface corresponds to this sag:

$$R = \frac{l^2}{8f} = \frac{130^2}{8 \cdot 3} = 700 \text{ mm}.$$

Evaluating the stretching voltage σ in the chamber walls by the formula known from the resistance of materials we obtain

$$\sigma = \frac{p \cdot R}{\varsigma} = \frac{1 \cdot 1700}{0.5} = 1400 \text{ kg/mm}^2.$$

The yield stress for the steel 12X18H10T is σ_T = 2200 kg/cm², i.e. the strength margin is

$$\frac{\sigma_T}{\sigma} = \frac{2200}{1400} = 1.6.$$

The chamber input water-cooled flange has an aperture of 80 mm in diameter, two copper inserts **7** , which are soldered to the flange. The inserts protect the chamber thin walls from the low energy and reflect3ed electrons. At the same time, they displace from the chamber a fraction of the magnetic flux thereby decrease the heating of the scanning chamber walls.

The scanning magnet has a sectioned magnetoguide with two pairs of coils on it. The magnetic guide of the crossection 100x40 mm consists of four parts and assembled of 0.35 mm thick electrotechnical steel and impregnated by the epoxy compound by the «Monolyth» technique.

Scanning magnet parameters:

1. Scanning angle $\pm 25°$.
2. Magnetic field in a gap   900 Gauss.
3. Total ampereturns of coils   5500 A.
4. Coil inductance   25 mHr.
5. Operation voltage of coil   2000 V.

For the time of 500 mks, the scanning magnet is scanning the electron beam along the converter of 1 m in length.

The Panoffsky lens is made in the form of two rectangular plates of 1150 mm in length and crossection 100x30 mm^2 made of a magnetic steel. There are 1500 turns on each plate.

The ends of plates are fixed between each other by the nonferrous strips and hanged to the bracket **2** , which holds the whole extraction window.

The converter (see Fig.17) is a bremsstrahlung target consisting of the aluminum plated with channels for cooling water, to which a 1 mm thick tantalum
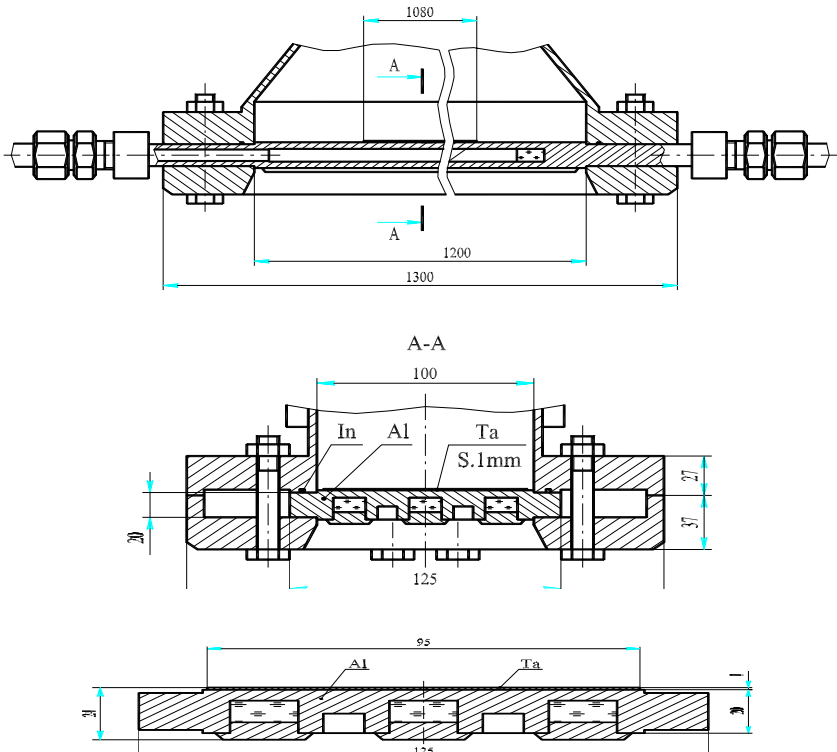
Fig. 17. Design of the gamma-converter for ILU-10 accelerator.

plate is welded by the explosion welding technique. According to calculations, at an energy of 5 MeV at tantalum thickness of 0.9 mm a fraction of gamma radiation outgoing from the converter is 5% of the beam power and the fraction of the reflected energy in the form of gamma radiation is ~ 15%. The remaining part of the beam power heats the tantalum plate operative surface. At an angle of incidence of electrons onto the target is $90°$ and the converter operative length is ~ 800 mm. Therefore, the specific thermal load to the target is

$$\frac{50 \cdot 0.8 \cdot 10^3}{80 \cdot 10} = 50 \text{ W/cm}^2 \quad .$$

Cooling channels inside the aluminum plate enable the water flow passage of 30 l/min at the pressure drop of 1.34 atm. At such water consumption, the heat transfer coefficient is ~1.6 W/cm^2°C and this is enough for removing heat from the converter.

3.2 Design of the extraction device for KSEA

The 3extraction foil is made as an individual unit of the extraction device (Fig.18). The unit with a foil (D-D crossection) is assembled separately, vacuum tight tested and bolted to the flat rectangular flange of the bellhood. The indium wire of 0.8 mm in diameter is used as a seal. The window itself is made of $\delta = 80 \, \mu m$, thick titanium with a specially made cylindrical form of 150 mm in radius.

Under atmospheric pressure, the foil is stretched and has tenses:

$$\sigma = \frac{P \cdot R}{\delta} = \frac{1 \cdot 150}{0.08} = 1870 \text{ kg/cm}^2 .$$

For the titanium alloy BT-1, which is used for producing foil, the strength limit at the operative temperature $200°C$ is $\sigma_e = 2850 \text{ kg/cm}^2$, i.e. the strength margin is $\frac{2850}{1870} = 1.52$.

The foil is vacuum tight fixed between two frames with bolts and spring washers. The seal here is a 0.8 mm thick indium wire. The frame has a water cooled channel protecting against overheating both indium seals in the process of work and during preliminary de-gassing heating of the extraction device.

During the passage of the electron beam through a 80 mkm thick foil, the energy loss is 55 keV. At an electron beam pow3er of 50 kW and mean current of 10 mA, the heat released on the foil is of 5530 W. This heat is removed by the arranged air flux at a speed of 20 m/s. To this end, the nozzle connected to the compressed air channel is installed along the window.
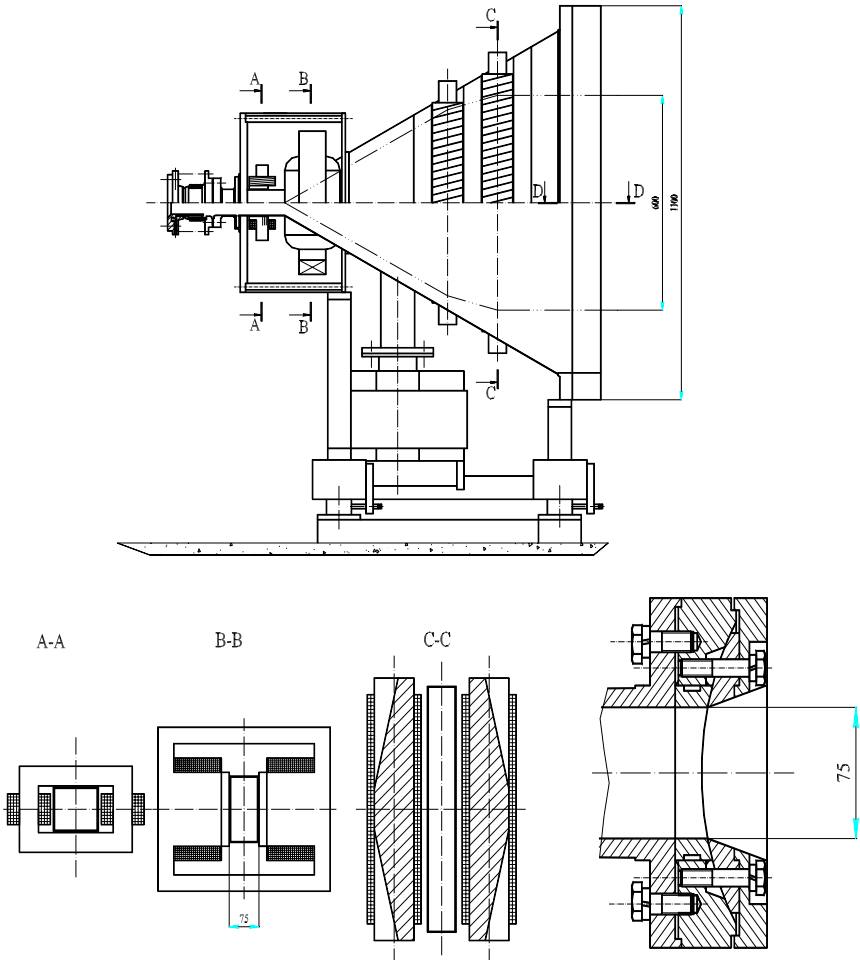
Fig. 18. Extraction device for KSEA accelerator.

4. Longitudinal scanning of an electron beam

When an electron is moving in the scanning magnet field (see Fig.19), at any current moment, the following expression is valid:

$$\sin\varphi = \frac{a_\varphi}{R} = \frac{a_0 \cdot F(\varphi)}{R}, \tag{4.1}$$

where a_φ is a design current length of the magnetic field, m;

   R is the circle radius m , determined by the known expression

$$\beta(E + E_0) = 375 H(t)\cdot R \ ,$$

E is the electron kinetic energy in terms of eV, $E_0 = 0{,}511 \cdot 10^6$ eV;

$H(t)$ is the magnetic field, A/m; $\beta = \dfrac{\nu}{c}$, where ν is the electron velocity, c is the speed of light.
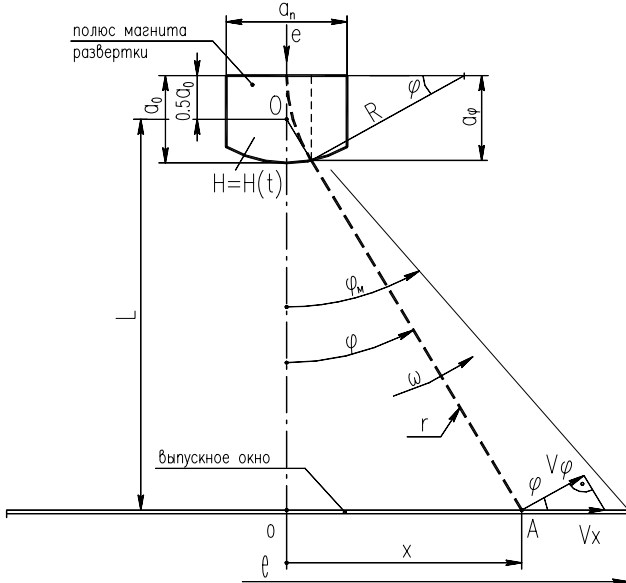
Fig. 19. Schematic of the electron beam scanning.

The geometric expression (4.1) is well followed if the magnet pole sizes $a_n \times a_n$. For the values $\dfrac{\delta}{a_n} = 0.25 \div 1$ the design length of the field is determined by the approximate expression:

$$a_0 \approx a_n (1 + 0.8\frac{\delta}{a_n}) .$$

By substituting R into (1) we obtain

$$\frac{\sin\varphi}{a_\varphi} = \frac{\sin\varphi}{a_0 \cdot F(\varphi)} = \frac{375}{\beta(E+E_0)} \cdot H(t) \ . \tag{4.2}$$

Multiplying the parts of equation by a_0 and introducing the designation $H_0 = \dfrac{\beta(E + E_0)}{375a_0}$, we have

$$H(t) = H_0 \frac{\sin \varphi}{F(\varphi)}, \tag{4.3}$$

where H_0 is a virtual intensity of the field at $R = a_0$ and $\sin \varphi_0 = 1$.

By differentiating the expression (4.2), we find out the beam angular velocity $\omega = \dfrac{d\varphi}{dt}$ around the rotation center – the point «0» in Fig. 19.

$$\frac{\cos \varphi \cdot a_\varphi - a_\varphi' \cdot \sin \varphi}{a_\varphi^2} \cdot d\varphi = \frac{375}{\beta(E + E_0)} \cdot H'(t) \cdot dt ,$$

whence

$$\omega = \frac{375}{\beta(E + E_0)} \cdot \frac{a_\varphi^2}{\cos\varphi \cdot a_\varphi - a_\varphi' \cdot \sin\varphi} \cdot H'(t) = \frac{a_\varphi}{(\cos\varphi - \dfrac{a_\varphi'}{a_\varphi} \cdot \sin\varphi) \cdot a_0} \cdot \frac{H'(t)}{H_0} \tag{4.4}$$

The beam velocity along the extraction window foil (see Fig.19) will be:

$$V_x = \frac{V_\varphi}{\cos\varphi} = \frac{r \cdot \omega}{\cos\varphi} = \frac{L}{\cos^2 \varphi} \, \omega . \tag{4.5}$$

4.1 Scanning of an electron beam at linear dependence of H(t)

Let us consider three versions of the scanning magnet poles with the power supply of the magnet windings by the saw wise current with a period T:

1. $a_\varphi = a_0 = \text{const}$

2. $a_\varphi = \dfrac{a_0}{\varphi} \cdot \sin \varphi$

3. $a_\varphi = a_0 \cdot \cos \varphi$

Using expressions (4.2), (4.3), (4.4), (4.5), we define the basic dependencies for each magnet profile by the parameter a_φ.

Table 1 shows the calculation results at a linear dependence of $H(t)$.

Table 1

Magnet profile	$H(\varphi)$	$H(t)$	ω	V_x
$a_\varphi = a_0 = \text{const}$	$H_0 \cdot \sin\varphi$	$H_0 \sin\varphi_m \dfrac{4}{T} t$	$\dfrac{4}{T} \dfrac{\sin\varphi_m}{\cos\varphi}$	$\dfrac{4L}{T} \dfrac{\sin\varphi_m}{\cos^3\varphi}$
$a_\varphi = \dfrac{a_0}{\varphi} \sin\varphi$	$H_0 \cdot \varphi$	$H_0 \varphi_1 \dfrac{4}{T} t$	$\dfrac{4}{T} \varphi_m = \text{const}$	$\dfrac{4L}{T} \dfrac{\varphi_M}{\cos^2\varphi}$
$a_\varphi = a_0 = \text{const}\,\varphi$	$H_0 \cdot \text{tg}\,\varphi$	$H_0 \,\text{tg}\,\varphi_m \dfrac{4}{T} t$	$\dfrac{4}{T} \text{tg}\,\varphi_m \cos^2\varphi_m$	$\dfrac{4L}{T} \text{tg}\,\varphi = \text{const}$

For the considered cases, let us calculate the ratio of the beam velocity at the window edge and its center $\dfrac{V_x}{V_0}$, which characterizes simultaneously the nonuniformity of the density of the electron radiation extracted into air. The magnetic field variation law is taken to be linear. Calculation results of the velocity ratio V_x/V_0 are given in Table 2.

Table 2

№	Magnet pole profile	Beam deflection angle φ, degrees					
		15°	20°	30°	35°	40°	45°
1	$a_\varphi = a_0 = \text{const}$	1,11	1,2	1,54	1,82	2,22	2,83
2	$a_\varphi = \dfrac{a_0}{\varphi} \sin\varphi$ $\approx a_0\,(1 - \dfrac{\varphi^2}{6})$	1,07	1,13	1,33	1,49	1,7	2,0
3	$a_\varphi = a_0 \cdot \cos\varphi$	1	1	1	1	1	1

4.2 Electron beam scanning with $Vx = \text{const}$ at linear dependence H(t)

At the constant beam velocity we have $V_x = \dfrac{2l}{T}$, where l, T are the length and period of a symmetric saw like scanning.

On the other hand, $V_x = \dfrac{V_\varphi}{\cos \varphi} = r \cdot \omega = \dfrac{L}{\cos^2 \varphi} \cdot \omega$, whence and angular frequency

$$\omega = \frac{V_x \cos^2}{L} \varphi = \frac{2l}{LT} \cos^2 \varphi = \omega_0 \, \cos^2 \varphi \,, \tag{4.6}$$

where $\omega_0 = \dfrac{2l}{LT}$ - the beam angular frequency at $\varphi = 0$.

The bending angle at $V_x = const$ is equal to

$$\varphi = \operatorname{arctg} \frac{V_x}{L} t = \operatorname{arctg} \omega_0 t \quad \text{or} \quad \operatorname{tg} \varphi = \omega_0 t \,. \tag{4.7}$$

For each magnet profile, by the expression (4.4) we find out the angular frequency and equate it with ω by the expression (4.6) we obtain:

1. $a_\varphi = a_0$, $\qquad\qquad H'(t) = \omega_0 \cdot H_0 \cdot \cos^3 \varphi$ (4.8)

2. $a_\varphi = \dfrac{a_0}{\varphi} \sin \varphi$, $\qquad H'(t) = \omega_0 \cdot H_0 \cdot \cos^2 \varphi$ (4.9)

3. $a_\varphi = a_0 \cdot \cos \varphi$, $\qquad H'(t) = \omega_0 \cdot H_0$ (4.10)

By integration of expressions (4.8), (4.9), (4.10) we find out the dependence $H(t)$ for each version. Calculation results are given in Table 3.

Table 3

Magnet profile	$H(\varphi)$	$H(t)$	ω	φ	$H'(t)$
$a_\varphi = a_0 = \text{const}$	$H_0 \cdot \sin \varphi$	$H_0 \cdot \sin (\operatorname{arctg} \omega_0 t)$	$\dfrac{H'(t)}{H_0 \cdot \cos \varphi}$	$\operatorname{arctg} \omega_0\, t$	$\omega_0 H_0 \cdot$ $\cdot \cos^3 \varphi$
$a_\varphi = \dfrac{a_0}{\varphi} \sin \varphi$	$H_0 \cdot \varphi$	$H_0 \cdot \operatorname{arctg} \omega_0 t$	$\dfrac{H'(t)}{H_0}$	$\operatorname{arctg} \omega_0\, t$	$\omega_0 H_0 \cdot$ $\cdot \cos^2 \varphi$
$a_\varphi = a_0 \cdot \cos \varphi$	$H_0 \cdot \operatorname{tg} \varphi$	$H_0 \cdot \omega_0 t$	$\dfrac{H'(t)}{H_0} \cos^2 \varphi$	$\operatorname{arctg} \omega_0\, t$	$\omega_0 H_0$ $= const$

The approximately constant beam velocity V_x for the version 2 (the magnet edge is profiled by the curve $a_\varphi = \dfrac{a_0}{\varphi} \cdot \sin \varphi$, $\varphi_m < 45°$) one can get at more widely used expression $H_2(t) = H_{2m} \cdot \sin \omega_2 t$, where

$$\omega_2 > \frac{2\pi}{T} \quad \text{or} \quad H_{2m} > H_0 \cdot \varphi_1 \,. \tag{4.11}$$

25

The required value ω_2 is found out from the condition that the ratio of derivatives $\dfrac{H_2'(0.25T)}{H_2'(0)} = \cos^2 \varphi_m$ compensates for the nonuniformity of the beam velocities at the edges and in the center of the extraction window. By differentiating $H_2(t)$, we obtain

$$\cos \omega_2 \frac{T}{4} = \cos^2 \varphi_m ,$$

from where we define ω_2. $H_2(t)$ amplitude is defined from the equality of the field intensities at the time moment $t = T/4$, i.e.

$$H_{2m} = H_0 \cdot \varphi_m / \sin \omega_2 \frac{T}{4} .$$

Table 4 give the values of ω_2 and $H_{2i}(t)$ for various scanning angles φ_m and period $T = 1/50$ s.

Table 4

φ_m^o	20	25	30	35	40	45
ω_2	97.8	121	144.4	167	189	209.2
$f_2 = \omega_2/2\pi$	15.6	19.4	23	26.6	30.1	33.3
$f_2 \Big/ \dfrac{1}{T}$	0.31	0.39	0.46	0.53	0.6	0.67
$H_{2m}/ H_0 \cdot \varphi_m$	2.13	1.75	1.52	1.35	1.23	1.16

An approximately constant beam velocity one can also obtain for the magnet nonprofiled edge $a_\varphi = a_0$, for which the following ratio of derivatives $\dfrac{H_1'(0.25T)}{H_1'(0)} = \cos^3 \varphi_m$ is valid.

$H_1(t)$, amplitude is determined by the equality of the field intensities at $t = T/4$, i.e.

$$H_{1m} = H_0 \sin \varphi_m / \sin \omega_1 \frac{T}{4} .$$

Calculations results for ω_1 and $H_{1m}(t)$ for various scanning angles φ_m and period $T = 1/50$ s are given in Table 5.

Table 5

φ_m^o	20	25	30	35	40	45
ω_l	118.6	146.2	172.6	197.8	220	242
$F_l = \omega_l/2\pi$	18.9	23.3	27.5	31.5	35	38.5
$f_1 / \dfrac{1}{T}$	0.38	0.47	0.55	0.63	0.7	0.77
$H_{1m}/H_0 \cdot \sin \varphi_m$	1.8	1.5	1.32	1.2	1.12	1.07

4.3 Extraction device with a postbending magnet (Panoffsky lens)

At the incidence angle on the electron beam onto the target of 90 C, the maximum deflection angles φ_m and postbending angles φ_{1m} are equal, i.e. $\varphi_m = -\varphi_{1m}$.
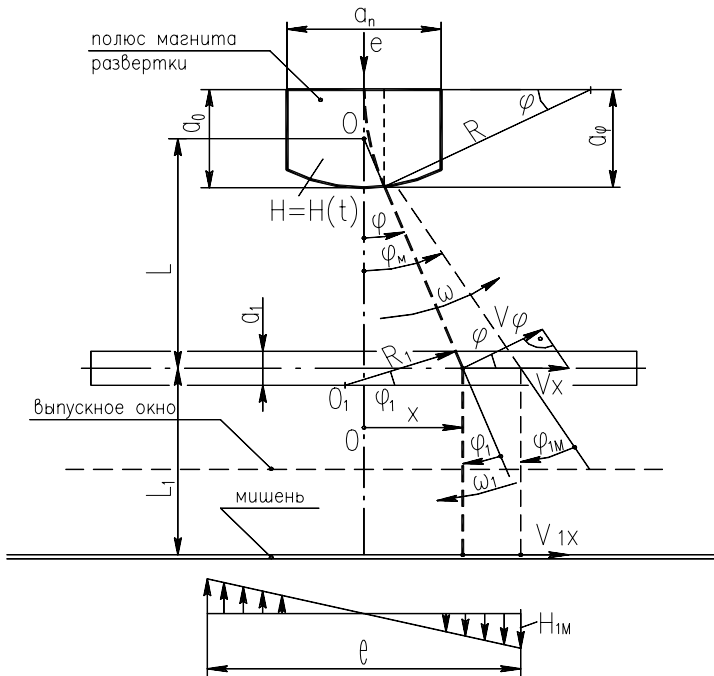
Fig. 20. Schematic of the electron beam scanning with a postbending magnet (Panoffsky lens).

For the electron motion in the field of the postbending magnet (Fig.20) the following expression is valid

27

$$\sin \varphi_1 = \frac{a_1}{R_1}, \tag{4.12}$$

where by the analogy with (4.1) we have $\beta(E + E_0) = 375 H_1(t) \cdot R_1$, in this case,

$$H_1(t) = \frac{4H_{1m}}{T} \cdot t,$$

where T is the period of the «saw-wise» scanning, H_{1m} is the maximum intensity of the magnetic field of the postbending magnet. H_{1m} is related to the scanning magnet intensity H_m by the following expression $H_{1m} a_1 = H_m a_0$, which is a consequence of the equality of angles $\varphi_m = -\varphi_{1m}$.

By substituting R_1 into (4.12) we obtain

$$\frac{\sin \varphi_1}{a_1} = \frac{375}{\beta(E + E_0)} \frac{4H_{1m}}{T} t \; .$$

By differentiation of the expression (4.12), we find out the beam angular velocity ω_1 around the rotation center-point O_1 in Fig.20.

$$\cos \varphi_1 \, d\varphi_1 = \frac{375 a_1}{\beta(E + E_0)} \frac{4H_{1m}}{T} dt = \frac{H_{1m}}{H_1} \cdot \frac{4}{T},$$

where:

$$\frac{d\varphi_1}{dt} = \omega_1 = \frac{H_{1m}}{H_1} \frac{4}{T} \frac{1}{\cos \varphi_1} \; .$$

The beam in the postbending magnet is rotated with an angular velocity of ω_1 to side opposite to that of ω scanning magnet. The beam angular velocity in a nonprofiled scanning magnet ($a_\varphi = a_0 = \text{const},$) at the saw-wise current in the magnet windings is equal to

$$\omega = \frac{H_{1m}}{H_1} \frac{4}{T} \frac{1}{\cos \varphi_1} \; .$$

In the case of $\varphi_m = \varphi_{1m}$, $a_0 H_m = a_1 H_{1m}$, the angular velocities are changed synchronously and $\omega = -\omega_1$ at any beam deflection angle and the beam velocity in the target is $V_{1x} = V_x$.

Therefore, the ratio of the beam velocities at the edge and in the center of the window in the presence of the Panoffsky lens is not changed and corresponds to the data given in Table 2.

Expressions obtained for $Vx = \text{const}$ and linear dependence $H(t)$ have been tested with PC and presented in Figs.21 and 22.
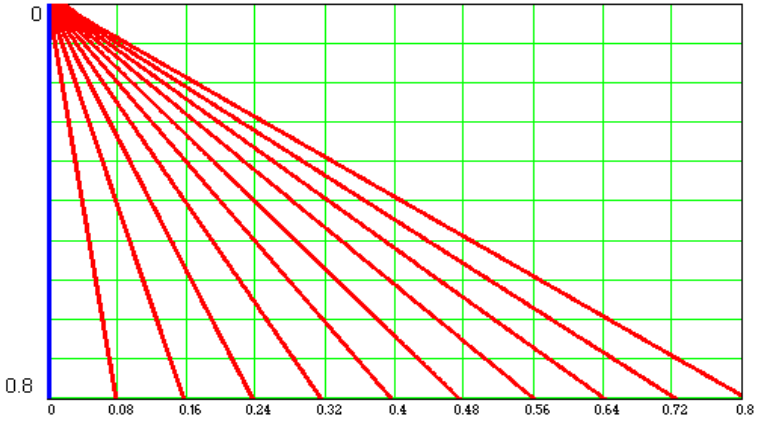
Fig. 21. The beam trajectory for the magnet edge profiled by the expression $a_\varphi = a_0 \cos\varphi$. *H(t)* is given discretely with the same step.
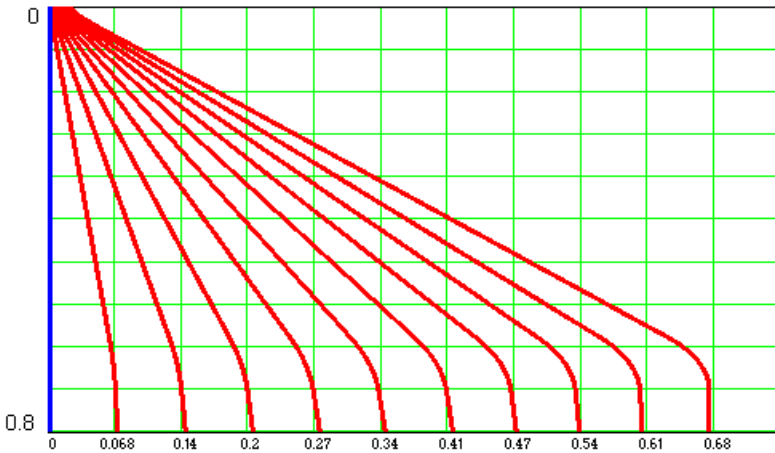
Fig. 22. The beam trajectory for the scanning magnet edge profiled by the expression $a_\varphi = a_0 \cos\varphi$ with the use of the postbending magnet (Panoffsky lens).

5. Electron-optical system for the electron beam extraction. Example of calculation

The first system of the electron beam formation in the ILU-10 accelerator after its acceleration in the cavity is the axisymmetric magnetic lens that is preparing the beam optimal parameters for its turn to 90 degrees. The bending system comprises five quadrupole lenses, two bending magnets and one corrector. The system is described in detail in [9]. The finish extraction system was selected to be the scheme, which consists of two electromagnets with one O-shaped core located either near the extraction window or the bremsstrahlung target of the flat quadrupole lens, which are scanning the beam in two planes. The total length of the extraction channel in vacuum is about 4 meters. Let us consider the main design problems for the electron-optical system of extraction devices.

5.1 Calculation of the space charge influence on the beam transportation

The differential equation of the edge electron for the laminar and paraxial beams with derivatives over the current coordinate $-(z)$ in the static electric and magnetic fields according [10] has the form:

$$r'' = \frac{\gamma'\gamma}{\gamma^2-1}r' \frac{8.6\cdot10^4}{\gamma^2-1}\left(B_z^2 - \left(\frac{r_k}{r}\right)^4 B_k^2\right)r \frac{0.5\gamma\gamma'}{\gamma^2-1}r + \frac{1.2\cdot10^{-4}\,I_e}{(\gamma^2-1)^{3/2}}\frac{1}{r}, \quad (5.1)$$

where: $r(z)$ – is the current radius of the edge electron,
B_z – is the magnetic field value at the axis,
B_k – is the magnetic field value at the cathode,
r_k – is the cathode radius,
I_e – is the beam current,
$\gamma(z)$ – is the relativistic factor.

Let us consider the beam transportation in ILU-10 after acceleration in the cavity for the case of motion of the lengthy flows with an account for only transverse component of the beam Coulomb charge. For another case, taking into account that $B_z = 0$, γ' and γ'' are also equal to zero, $B_k = 0$ by the condition of the beam formation in the cavity. In this case, the only final term is remaining in the right hand side of the equation [5.1]. The equation solution for this case shows that the flow expansion effect caused by the beam space charge can be neglected (at a length of 4 meters the beam is expanded only by 10%).

5.2 Calculation of the main electron-optical parameters of extraction devices

Further calculation of the beam motion will be performed with the method of trajectory analysis by solving a set of scalar equations for the Cartesian coordinates - the projection of the vector equation of electron motion in the magnetic field:

$$
\left.
\begin{array}{l}
\dfrac{d^2 x}{dt^2} = -\eta \left(B_z \dfrac{dy}{dt} - B_y \dfrac{dz}{dt} \right), \\[2mm]
\dfrac{d^2 y}{dt^2} = -\eta \left(B_x \dfrac{dz}{dt} - B_z \dfrac{dx}{dt} \right), \\[2mm]
\dfrac{d^2 z}{dt^2} = -\eta \left(B_y \dfrac{dx}{dt} - B_x \dfrac{dy}{dt} \right).
\end{array}
\right\}
\qquad (5.2)
$$

The magnetic poles of the extraction system along the X-axis (the wide side of the bellhood) are made rather lengthy and the magnetic fields along the coordinate have no specific features. This means that in the zone of beam availability in the bending magnetic, the field along the X-coordinate is the same and in the Panoffsky lens, the operating field gradient is constant.

The edge fields of the scanning magnet and quadrupole lens is approximated by the linear function. This form of approximation enable one to obtain the simple and easily analyzable expressions for the components of magnetic fields of the scanning device. It is worth to add that the realized ratio of the length and width of the bellhood magnetoguide, which was chosen, for example, for R.Korea (Fig.24) shows that such a kind of the linear approximation is rather evident.
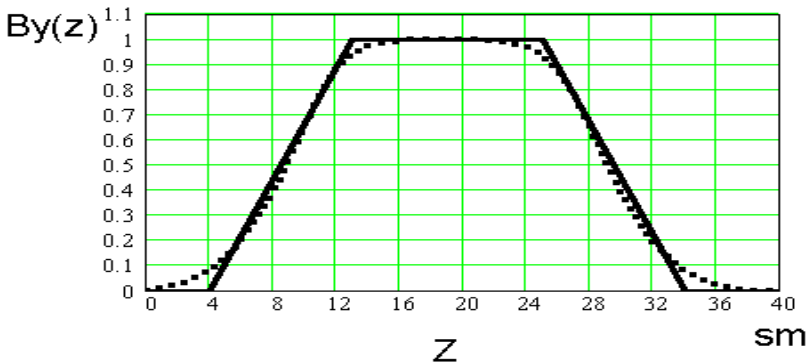
Fig. 24. The form of the real magnetic field of the bending magnet and its approximation function.

31

For this approximation, the magnetic field components with an account for the end fields according to [11] take the form:

$$
\left.
\begin{aligned}
B_x &= G(z)\cdot y \\
B_y &= G(z)\cdot x + B(z) \\
B_z &= G'(z)\cdot x \cdot y - \frac{1}{2}B'(z)
\end{aligned}
\right\} , \qquad (5.3)
$$

where $B(z)$ is the scanning magnet field distribution along the Z-axis, $G(z)$ is the magnetic field gradient distribution for the output Panoffsky lens

$$
\left(G = \frac{dB_x}{dx} = \frac{dB_x}{dy} \right), \text{ at } x = y = 0 .
$$

Fig.25 shows the result of calculations for the expanded beam trajectories of the monochromatic beam and the beam with an energy spread of the ILU-10 accelerator.

The beam is given at the input by the circle of points whose trajectories give a vivid three-dimensional image of the beam form deformation in the plane of the extraction device bellhood. The size along the Z-axis is chosen with a double margin.
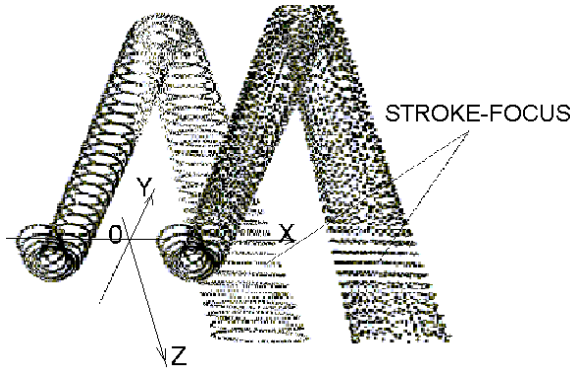
Fig. 25. The beam form transformation during its passage through the bellhood magnetic fields.

When considering in chapter 3 the problems of the dose fields formation at the output of the extraction devices, the size of the beam along the bellhood narrow side (Y-axis) is was taken to be constant.

Let us consider in more detail the problem of obtaining the required beam characteristics. The scanning magnet field is produced with the magnetic poles

rather lengthy along the longitudinal scanning coordinate. In this region, according to [12] the field of spread at the pole edges plays the role of a cylindrical lens, which can substantially deform the beam transverse size in the direct dependence on the scanning alternative field. For example, the design ratio of the transverse size to the maximum deviation and without it in the absence of the output quadrupole lens for the ILU-10 optical system was achieved to be 1.7. With the use of the flat quadrupole lens as a postbending device, the beam transverse size was managed practically to be fixed. Fig.26 shows the beam transverse size of the ILU-10 accelerator at the zeroth and maximum deviations.
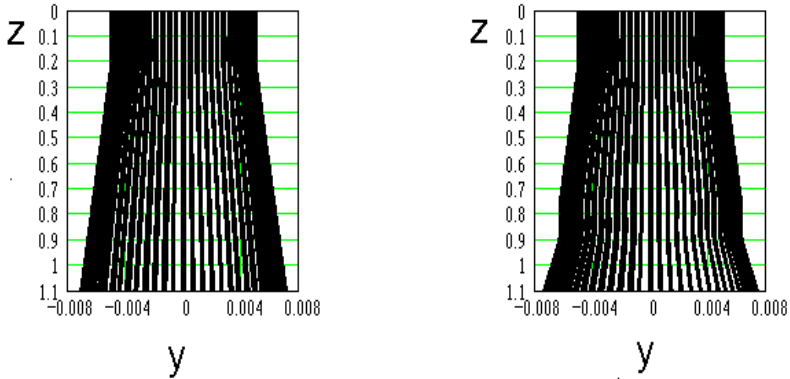
Fig. 26. Projection of the ILU-10 beam onto the narrow side of the bellhood.

The experiment proved that the beam transverse size in ILU-10 accelerator with an output quadrupole lens along the entire required length of scanning is constant. Fig.27 shows the beam transverse size of the beam of the ILU-10 accelerator.
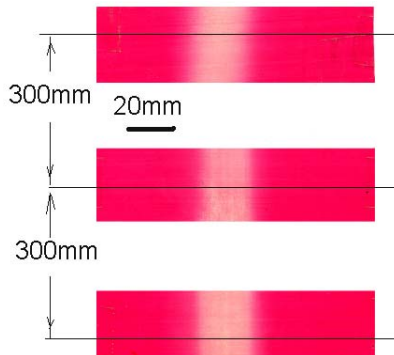
Fig. 27. The electron beam trace behind the foil of ILU-10 accelerator.

33

In conclusion, let us note that the beam extraction system designed by this techniques for the ILU-10 accelerator enabled us to obtain the required dose parameters (Fig.28). The long-term tests have shown the high reliability and a comparative simplicity of the extraction device. The beam extraction system for the KSEA acceleration was put into production.
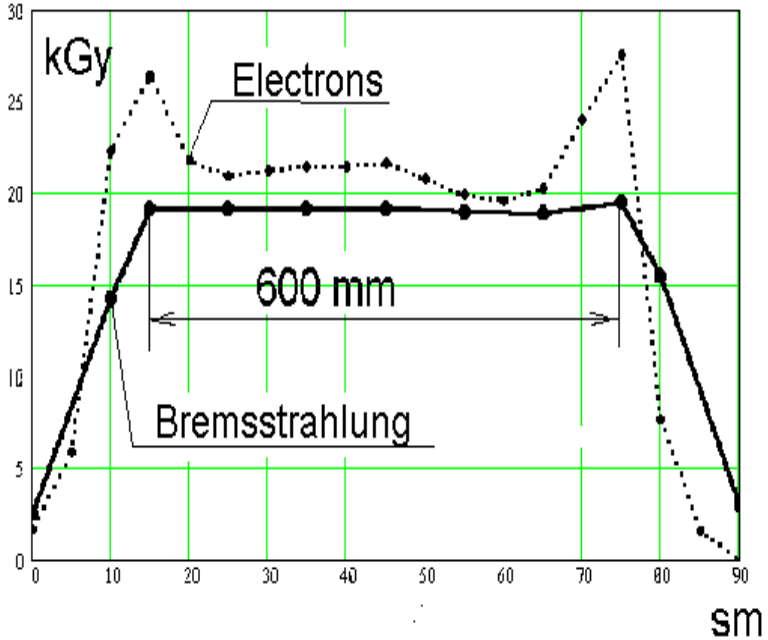
Fig. 28. Distribution of the dose parameters of the ILU-10 extraction system.

Literature

[1] Kuksanov N.K., Salimov R.A., Cherepkov V.G. *Extraction into air of the scanned electron beam with a current up to 100 mA.*- PTE N4, 1988.

[2] Svinin M.P. *Calculation and design of high voltage electron accelerators for radiation technologies.* – M.: Energoizdat, 1989.

[3] Auslender V.L. et al*., A pulse high frequency linear accelerator of electrons ILU-10.* Novosibirsk, 2002 (Vestnik «RADTECH-EURASIA»; № 1 (11)).

[4] Vasiliev V.V. et al.*Conducting shells in a pulsed electromagnetic field.* – M.: Energoatomizdat, 1982.

[5] Golubenkov Yu.I., M.E. Veis, N.K. Kuksanov et al. *Accelerators of ELV-type: status, development, applications.* Novosibirsk, 1999 (Vestnik «RADTECH-EURASIA»; № 2 (10)).

[6] Krug K.A. *Electrotechnic Fundamentals.* – M.1936.

[7] Ginzburg S.G. *Methods for solution of transition processes in electric circuits.* – M.: Higher School, 1967.

[8] Auslender V.L. et al. *A system for measuring the dose power and its spatial distribution in power bremsstrahlung radiation in the regime «on-line».* Novosibirsk, 2002 (Vestnik «RADTECH-EURASIA»; № 1 (11)).

[9] Auslender V.L. et al. *An achromatic system for 90 degrees bending of the electron beam in the ILU-10 accelerator.* Sankt-Petersburg, 2001, Proceedings of the 10th International Meeting on the use of the charged particle accelerators in industry and medicine.

[10] Wasserman S.B. et al. *Optics of the accelerator tube of the electron beam generator of ELIT-3A accelerator.* Preprint BINP № 85-28, Novosibirsk, 1985

[11] Kotov V.I., Miller V.V. *Focusing and mass distribution of high energy particles.* - M.: Atomizdat, 1969.

[12] Kelman et al. *Electron-optical components of the prism spectrometers of charged particles.* - Alma-Ata.: Nauka, 1979.

В.Л. Ауслендер, А.В. Булатов, Л.А. Воронин, Д.С. Колесников,
Е.Н. Кокин, Г.С. Крайнов, А.Н. Лукин, А.М. Молокоедов,
В.М. Радченко, Н.Д. Ромашко

Методика расчета и конструирования выпускных устройств
для ускорителей электронов

V.L. Auslender, A.V. Bulatov, L.A. Voronin, D.S. Kolesnikov,
E.N. Kokin, G.S. Krainov, A.N. Lukin, A.M. Molokoedov,
V.M. Radchenko, N.D. Romashko

Technique of design and calculation of extraction devices
for electron accelerators

Budker INP 2004-27